Bio-Design and Manufacturing (2025) 8:625–638
https://doi.org/10.1631/bdm.2400339

RESEARCH ARTICLE

A redox-responsive nanovaccine for cytosolic delivery of antigen and adjuvant to enhance cancer immunotherapy

Taisheng Liu[1] · Bingkai He[2] · Jiaqing Tao[2] · Shaoying He[2] · Nanlin Fu[3] · Kewei Wang[4,5] · Hui Fan[2]

Received: 23 August 2024 / Accepted: 1 February 2025 / Published online: 22 May 2025

Abstract

Cancer vaccines have garnered significant attention in cancer immunotherapy because they trigger tumor-specific immune responses. However, their effectiveness is hindered by inefficient antigen and adjuvant delivery at the subcellular level, which is essential to stimulate a robust $CD8^+$ T cell response. This study presents PAR/OVA, a cancer nanovaccine developed by combining imiquimod (R837)-modified polyamidoamine dendrimers with the model protein antigen ovalbumin (OVA). Within the nanovaccine, R837 is an adjuvant for the Toll-like receptor 7 (TLR7) pathway and a structural component that facilitates OVA loading. In dendritic cells (DCs), the high cytoplasmic glutathione levels triggered the breakdown of PAR/OVA, releasing OVA and R837, which induced DC activation and antigen cross-presentation. Furthermore, PAR/OVA vaccination showed a protective effect and effectively inhibited B16-OVA tumor progression, indicating its potential in cancer immunotherapy. Combining this vaccine with an immune checkpoint blockade enhanced antitumor efficacy by improving the ability of cytotoxic T lymphocytes to target cancer cells within the tumor microenvironment. These findings underscore the potential of this adjuvant/antigen-delivering nanovaccine in cancer immunotherapy.

✉ Kewei Wang
wangkw@jnu.edu.cn

✉ Hui Fan
fanhui@gdpu.edu.cn

[1] Laboratory Animal Center, Guangdong Pharmaceutical University, Guangzhou 510006, China

[2] School of Pharmacy, Guangdong Pharmaceutical University, Guangzhou 510006, China

[3] School of Traditional Chinese Medicine, Guangdong Pharmaceutical University, Guangzhou 510006, China

[4] Key Laboratory of Biomaterials of Guangdong Higher Education Institutes, Department of Biomedical Engineering, Jinan University, Guangzhou 510632, China

[5] Guangdong Provincial Key Laboratory of Spine and Spinal Cord Reconstruction, The Fifth Affiliated Hospital of Jinan University (Heyuan Shenhe People's Hospital), Jinan University, Heyuan 517000, China

Graphical abstract

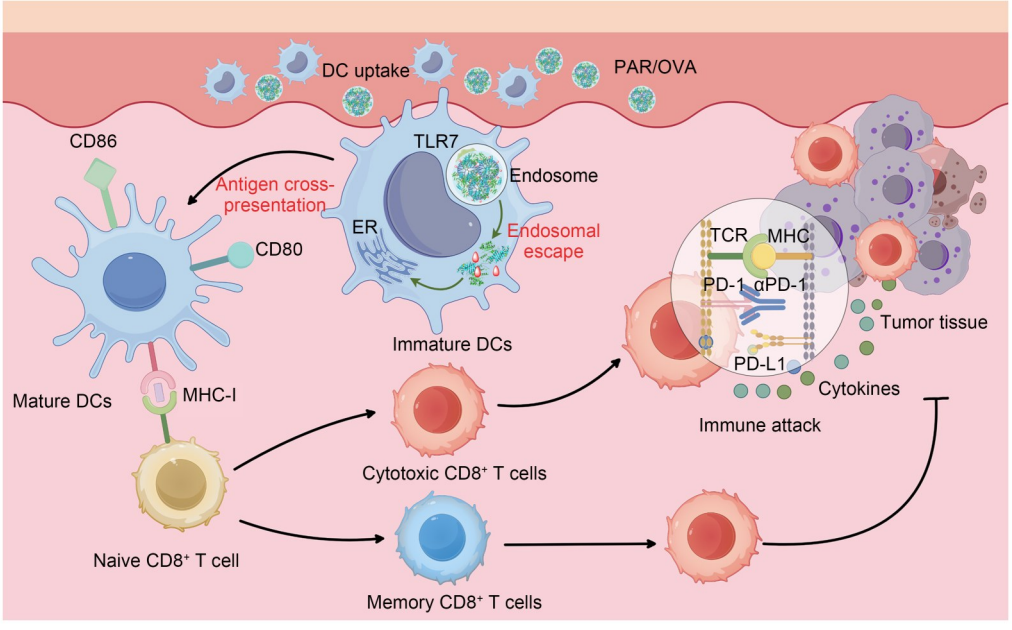

Keywords Nanovaccine · Cancer immunotherapy · Redox-responsive polymer · Cytosolic delivery · Synergistic therapy

1 Introduction

Cancer immunotherapy harnesses patients' immune systems to inhibit tumor proliferation and is widely recognized as an effective cancer treatment approach [1–3]. Several strategies, including immune checkpoint blockade (ICB), chimeric antigen receptor (CAR)-T cell therapy, and cancer vaccines, have been extensively studied and implemented in clinical practice [4, 5]. Therapeutic tumor vaccines, which can induce long-lasting and tumor-specific immune responses, are gaining significant attention in cancer research [6–8]. Unlike conventional vaccines designed for disease prevention, therapeutic vaccines are engineered to activate antigen-specific cellular immunity, enabling the targeted destruction of tumor cells. This process involves dendritic cells (DCs) internalizing exogenous antigenic proteins, resulting in antigen cross-presentation. This mechanism is essential for presenting exogenous antigens on major histocompatibility complex class I molecules, thereby boosting cellular immunity [9, 10]. Vaccine adjuvants and carriers can improve cross-presentation and foster the development of strong antigen-specific cellular immunity. However, the efficient delivery of antigens and adjuvants at the subcellular level remains a significant challenge [11].

Developing effective cytosolic delivery systems has garnered growing interest due to their essential role in cross-presentation. To enhance the cytosolic delivery of antigens and adjuvants, various cationic polymers and inorganic nanoparticles (NPs) have been explored as carriers, using the proton sponge effect, membrane fusion peptides, and pore-forming agents to achieve lysosomal escape of exogenous antigens [12–14]. Most of these carriers interact with antigens and adjuvants through electrostatic or hydrophobic forces, forming unstable complexes under physiological conditions [15]. Therefore, developing materials with improved stability is crucial for efficiently delivering antigens and adjuvants to the cytosol.

Recent studies have extensively explored polyamidoamine (PAMAM) dendrimers, demonstrating their efficacy as carriers for various biomolecules, including nucleic acids, proteins, and peptides [16]. The abundant amine groups on the surface of PAMAM dendrimers facilitate easy functionalization. Furthermore, the interior tertiary amino groups, with a pKa of approximately 6.5, can be protonated under mildly acidic conditions, promoting efficient endosomal escape and subsequent cytosolic delivery [15]. Surface modification of PAMAM dendrimers with hydrophobic groups offers several advantages, including payload compaction, increased cellular uptake, and enhanced biocompatibility [17–19]. For example, Xu et al. developed a PAMAM dendrimer grafted with guanidinobenzoic acid, which effectively binds ovalbumin (OVA) and disrupts endosomes [19]. Similarly, Gao et al. developed an effective cancer vaccine through multiple interactions among manganese ions, benzoic acid-modified

PAMAM dendrimer, and OVA [11]. These hydrophobically modified PAMAM dendrimers interact with cargo proteins through multiple interactions, enhancing the stability of the resulting complex and promoting efficient cytosolic delivery.

Imiquimod (R837) is essential for activating innate and adaptive immunity and has been approved by the United States Food and Drug Administration as an immunoadjuvant for treating cancers and viral infections [20–22]. As a Toll-like receptor 7 (TLR7) agonist, R837 triggers an immune response by inducing cytokine production in immune cells, promoting splenocyte proliferation, and facilitating DC maturation [23, 24]. However, the poor solubility and unfavorable pharmacokinetics of the small molecule R837 limit its clinical application [25]. To address these challenges, NP-based carriers have been explored for R837 delivery, including poly(lactic-co-glycolic acid) NPs [26, 27], $MnFe_2O_4$ NPs [28], and mesoporous silica NPs [29]. However, in these studies, R837 was predominantly encapsulated physically within NPs, which often resulted in low loading efficiency and premature release, presenting significant challenges for effective loading and controlled release in nanovaccine formulations.

In this study, we synthesized an R837-modified fourth-generation (G4) PAMAM dendrimer, termed PAR, to act as a carrier for the protein antigen OVA in the development of a nanovaccine (Scheme 1a). In the resulting PAR/OVA nanovaccine, R837 served as both a TLR7 adjuvant and a key facilitator of OVA loading and nanovaccine assembly. The PAR/OVA nanovaccine enhanced the uptake of both antigens and R837 by antigen-presenting cells. When PAR/OVA entered the acidic endosomal compartment, the reduced pH activated the endosomolytic action of the carrier, enabling PAR/OVA to escape into the cytosol (Scheme 1b). High glutathione (GSH) levels in the cytoplasm led to the breakdown of PAR/OVA, releasing OVA and R837, which activated DCs and facilitated antigen cross-presentation. The PAR/OVA nanovaccine was tested for both prophylactic and therapeutic efficacy in B16-OVA tumor models, with results significantly outperforming alternative treatments.

2 Materials and methods

2.1 Materials and characterization

The G4 PAMAM dendrimer was purchased from Weihai Chenyuan Co., Ltd. (Shandong, China). R837 was obtained from MedChemExpress LLC (USA). Bis(2-hydroxyethyl) disulfide and *p*-nitrophenyl chloroformate (NPC) were purchased from Energy Chemical (Shanghai, China). All other

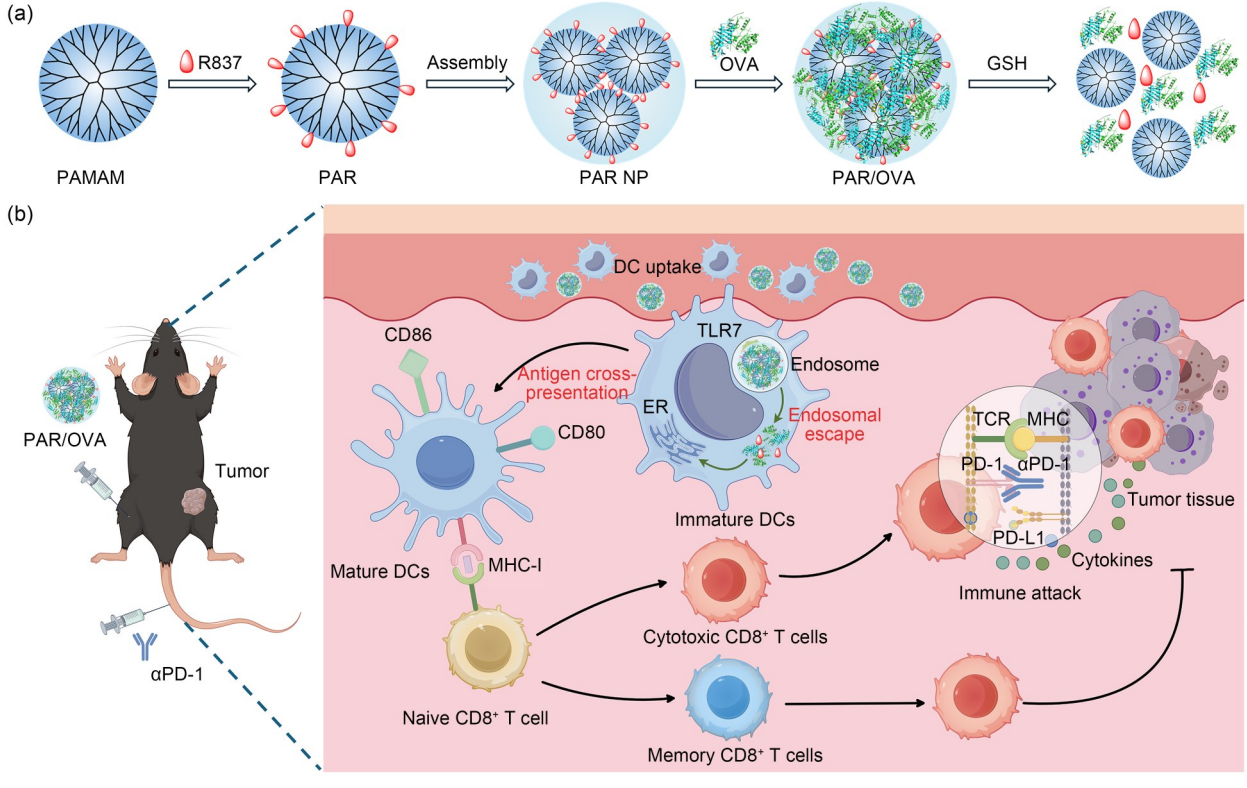

Scheme 1 A schematic illustration of the PAR/OVA preparation process (a) and its antitumor mechanism (b). TLR7: Toll-like receptor 7; αPD-1: anti-programmed cell death 1; MHC-I: major histocompatibility complex class I; ER: endoplasmic reticulum; TCR: T cell receptor; PD-L1: programmed cell death ligand 1

chemicals used in the experiments were purchased from Sigma-Aldrich Co., LLC (Shanghai, China) and used without further purification.

The nuclear magnetic resonance (NMR) spectra were measured with a Bruker ARX 400 NMR spectrometer (Billerica, MA, USA) using deuterated dimethyl sulfoxide (DMSO) as the solvent. Particle size and size distribution were measured in an aqueous solution using a Malvern ZS90 dynamic light scattering (DLS) instrument (Malvern Instruments Ltd., UK). Confocal images were acquired using a confocal laser scanning microscope (CLSM, ZEISS LSM880, Germany).

2.2 Cell lines and animals

The melanoma cell line B16-OVA and mouse dendritic cell line DC2.4 were obtained from the American Type Culture Collection (ATCC) and cultured in RPMI-1640 medium (Gibco, Thermo Fisher Scientific, MA, USA) supplemented with 10% (volume fraction) fetal bovine serum (FBS) in a 5% CO_2 atmosphere at 37 °C. Female C57BL/6 mice (5–6 weeks old) were purchased from Hunan SJA Laboratory Animal Co., Ltd. (Hunan, China).

2.3 Synthesis of PAR

Under an N_2 atmosphere, bis(2-hydroxyethyl) disulfide (154.0 mg, 1.0 mmol) was dissolved in CH_2Cl_2 (5.0 mL). NPC (504.0 mg, 2.5 mmol) and triethylamine (303.0 mg, 3.0 mmol) were added to the solution. The mixture was stirred for 2 h, followed by the addition of R837 (240.0 mg, 1.0 mmol). After stirring for an additional 12 h, the solvent was removed under reduced pressure. The crude product was purified using silica gel flash chromatography with a dichloromethane/methanol gradient (60∶1 to 10∶1), yielding Product 1 with an 85% yield. The PAMAM dendrimer (100 mg, 1 equiv) and Product 1 (82.4 mg, 20 equiv) were dissolved in anhydrous DMSO under an N_2 atmosphere and stirred overnight. After the reaction, the mixture was dialyzed using a 3500-Da molecular weight cutoff (MWCO) membrane, first against DMSO and then against ultrapure water. The solution was then lyophilized, resulting in a final yield of 78%.

2.4 Preparation and characterization of PAR/OVA

PAR (10 mg) was dissolved in 0.5 mL of DMSO and slowly added to 5 mL of water while stirring for 1 h. The mixture was transferred to a dialysis bag (MWCO: 3500 Da) and dialyzed against ultrapure water for 24 h to remove the DMSO, resulting in PAR NPs. The PAR NPs were mixed with OVA in water, vortexed, and incubated for 10 min to form PAR/OVA. The size and zeta potential of the prepared complexes were analyzed using DLS.

2.5 Determination of OVA loading efficiency

To determine the OVA loading efficiency, PAMAM/OVA and PAR/OVA were placed in an ultrafiltration tube with 100 kDa MWCO and centrifuged. The filtrate was collected, and the OVA concentration was determined using an enhanced bicinchoninic acid (BCA) protein assay kit (Beyotime, China) according to the manufacturer's instructions. These data were then used to estimate the OVA loading in the nanovaccines.

2.6 Cellular uptake and intracellular localization of OVA

The cellular uptake and intracellular localization of the vaccine formulations were assessed in DC2.4 cells using flow cytometry and confocal microscopy. DC2.4 cells were seeded in 24-well plates at a density of 1×10^5 cells/well and incubated overnight at 37 °C. The cells were then treated with Cyanine 5 (Cy5)-labeled OVA (OVA-Cy5), PAMAM/OVA-Cy5, OVA-Cy5+R837, or PAR/OVA-Cy5 (OVA-Cy5 concentration: 5 μg/mL) for 4 h. After washing three times with phosphate-buffered saline (PBS), the cells were trypsinized and collected for the analysis of cellular uptake using a flow cytometer (BD, Biosciences, USA).

To assess the intracellular localization of OVA, DC2.4 cells were seeded into laser confocal plates (diameter: 20 mm) at a density of 2×10^6 cells/dish and incubated overnight. The cells were treated with PAR/OVA-Cy5 (OVA-Cy5 concentration: 5 μg/mL) for 2, 4, and 8 h to assess endosomal escape. After a 30-min incubation with LysoTracker Green (200 nmol/L), the nuclei were stained with Hoechst 33342. Following three washes with PBS, the cells were imaged using CLSM.

2.7 Cytotoxicity assessment of PAR/OVA

The in vitro cytotoxicity of PAR/OVA was assessed using the Cell Counting Kit-8 (CCK-8) assay. DC2.4 cells were seeded into 96-well plates at a density of 1×10^4 cells/well and incubated overnight. After removing the culture medium, RPMI-1640 medium containing PAR/OVA at varying concentrations (0, 0.75, 1.5, 3, 6, 12, and 24 μg/mL OVA) was added, followed by a 24-h incubation. The cells were then treated with 10 μL of CCK-8 solution and incubated for another 4 h. Absorbance at 490 nm was then measured using a microplate reader (Biotek, Thermo Fisher Scientific).

2.8 In vitro DC maturation and cross-presentation assay

Immature bone marrow-derived DCs (BMDCs) (2×10^5 cells/well) were seeded into 24-well nontreated plates and stimulated with PBS, OVA, PAMAM/OVA, OVA+R837, or

PAR/OVA (OVA concentration: 10 μg/mL) for 24 or 48 h. After treatments, BMDCs were harvested, resuspended in PBS buffer containing 0.1% bovine serum albumin (BSA), incubated with anti-CD16/32 at 4 °C for 15 min, and stained with anti-CD11c-FITC (fluorescein isothiocyanate), anti-CD86-APC (allophycocyanin), and anti-CD80-PE (p-phycoerythrin) for 25 min. The cells were analyzed using flow cytometry. The supernatant was collected to measure tumor necrosis factor-alpha (TNF-α) and interleukin-6 (IL-6) levels using an enzyme-linked immunosorbent assay (ELISA) kit (Gilead Biotechnology, China) following the manufacturer's instructions.

For cross-presentation analysis, immature BMDCs (2×10^5 cells/well) were seeded into 24-well nontreated plates and stimulated with PBS, OVA, PAMAM/OVA, OVA+R837, or PAR/OVA (OVA concentration: 10 μg/mL) for 24 or 48 h. After treatments, the cells were harvested, resuspended in PBS buffer containing 0.1% BSA, incubated with anti-CD16/32 at 4 °C for 15 min, and stained with anti-CD11c-FITC and anti-SIINFEKL-H-2Kb-PE at 4 °C for 25 min. The cells were analyzed using flow cytometry.

2.9 Prophylactic and therapeutic trials of nanovaccines

In the prophylactic trial, female C57BL/6 mice in each group received one of the following vaccine formulations: OVA, PAMAM/OVA, OVA+R837, or PAR/OVA through subcutaneous injection at weekly intervals for three doses. Seven days after the final vaccination, the mice were subcutaneously challenged with 3.5×10^5 B16-OVA cells. Tumor volume was measured every other day using calipers and calculated as

$$V=lw^2/2,$$

where l represents the length (in mm) and w represents the width (in mm). The mice were euthanized when the tumor volume reached 2000 mm^3.

In the therapeutic trial, female C57BL/6 mice (six weeks old) were subcutaneously injected with 3.5×10^5 B16-OVA cells. Once the tumor volume reached approximately 80 mm^3, the mice were randomly divided into five groups (n=6) and administered subcutaneous vaccinations with one of the following formulations: OVA, PAMAM/OVA, OVA+R837, or PAR/OVA. Tumor volume and body weight were recorded every other day. On Day 26, the mice were euthanized for immunological analysis.

2.10 Therapeutic study in combination with anti-programmed cell death 1 (αPD-1)

In the combination therapy study, female C57BL/6 mice (six weeks old) were subcutaneously injected with 5×10^5 B16-OVA cells. Once the tumor volume reached approximately 80 mm^3, the mice were randomly assigned to five groups (n=6). Each group received subcutaneous vaccinations with PBS, OVA, PAMAM/OVA, OVA+R837, or PAR/OVA on Days 6, 13, and 20 post-tumor implantation. Additionally, αPD-1 was administered intravenously at a dose of 20 μg per mouse following each vaccination.

2.11 Statistical analysis

Data are presented as mean±standard deviation. Statistical comparisons between two groups were performed using Student's t-test, and one-way analysis of variance (ANOVA) was used for comparisons among multiple groups. The designation "ns" indicates nonsignificance. Statistical significance was set at $^{*}P<0.05$, $^{**}P<0.01$, and $^{***}P<0.001$.

3 Results and discussion

3.1 Preparation and characterization of PAR/OVA nanovaccine

PAR was synthesized by conjugating R837 to a G4 PAMAM dendrimer through GSH-sensitive disulfide bonds (Scheme S1 in the supplementary information), facilitating the release of R837 in the cytoplasm of antigen-presenting cells where GSH is abundant. The chemical structures of the product and intermediates were confirmed using ^{1}H NMR spectroscopy (Figs. S1 and S2 in the supplementary information). The synthesized PAR was insoluble in water, likely due to the high density of hydrophobic ligands on the PAMAM dendrimer. However, it was transformed into PAR NPs through a nanoprecipitation process, resulting in particles with a size of 50.6 nm (Fig. 1a). PAR NPs were then mixed with OVA in water via vortex agitation and incubated for 10 min to prepare the PAR/OVA nanovaccine, which exhibited a diameter of 198.2 nm and a spherical structure (Fig. 1b; Fig. S3 in the supplementary information). The PAR/OVA nanovaccine reduced the zeta potential of the PAR NPs from 37.3 to 12.4 mV (Fig. 1c).

The OVA loading efficiency of PAR/OVA was 88.3%, significantly higher than that of PAMAM/OVA (53.6%) (Fig. 1d). We then explored the role of R837 in the synthesis of the PAR/OVA nanovaccine. DLS analysis revealed that the PAMAM dendrimer had a particle size of approximately 5 nm and a zeta potential of +25.7 mV (Figs. S4a and S4c in the supplementary information). Due to the increased hydrophobicity, PAMAM-R837 self-assembled into larger PAR NPs in water (Fig. 1a). These PAR NPs exhibited a higher zeta potential (+37.5 mV) and GSH-triggered size reduction, along with a decrease in zeta potential (Figs. S4b and S4c in the supplementary information). Based on these findings, we hypothesized that electrostatic and hydrophobic interactions between PAR and OVA were key to OVA loading and PAR/OVA nanovaccine synthesis.

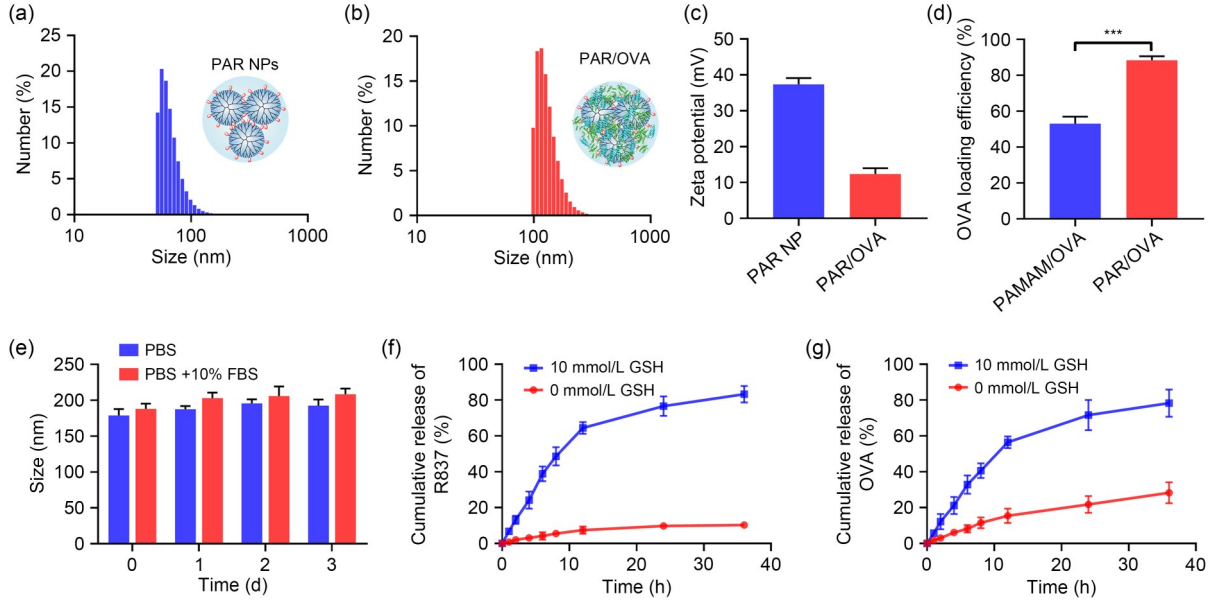

Fig. 1 Characterization of PAR/OVA nanovaccine. (a) Size distribution of PAR NPs measured using DLS. (b) Size distribution of PAR/OVA measured using DLS. (c) Zeta potentials of PAR NPs and PAR/OVA. (d) OVA loading efficiency of PAMAM/OVA and PAR/OVA. (e) Stability of PAR/OVA in PBS and PBS supplemented with 10% FBS. (f) R837 release profiles from PAR/OVA in the presence or absence of 10 mmol/L GSH. (g) OVA release profiles from PAR/OVA in the presence or absence of 10 mmol/L GSH. Data are presented as mean±standard deviation (n=3). Statistical significance was determined using the Student's t-test ($^{***}P<0.001$)

The stability of the PAR/OVA nanovaccine was assessed in both PBS and PBS supplemented with FBS. As shown in Fig. 1e, the particle size in both media remained relatively unchanged over the 72-h incubation period, indicating that the PAR/OVA nanovaccine was stable under physiological conditions. Furthermore, the release profiles of OVA and R837 were evaluated under simulated cytoplasmic conditions containing 10 mmol/L GSH. The results showed that R837 and OVA had similar release profiles at 10 mmol/L GSH (Figs. 1f and 1g), indicating coordinated release behavior.

3.2 Cellular uptake and intracellular localization of OVA

Cellular uptake of the different vaccines was quantified using flow cytometry. As shown in Figs. 2a and 2b, treatment with PAR/OVA resulted in a significantly higher mean fluorescence intensity (MFI) of OVA-Cy5 in DC2.4 cells than those in the OVA, PAMAM/OVA, and OVA+R837 groups. This enhanced cellular uptake of PAR/OVA could be attributed to the positive charge properties of PAMAM and the more efficient encapsulation of OVA by PAR NPs. The intracellular distribution of OVA-Cy5 in DC2.4 cells was further examined using CLSM. Figure 2c shows that the red fluorescence from OVA-Cy5 colocalized with the green signal from LysoTracker, indicating that OVA was effectively internalized by DC2.4 cells and transported to lysosomes. Extended incubation periods resulted in the separation of green and red fluorescence signals, with an increased presence of red signals in the cytoplasm, indicating a successful escape from endo/lysosomal compartments. Fluorescence colocalization analysis confirmed this, showing a decrease in Poisson's coefficient from 0.89 to 0.62 as the incubation time increased from 2 to 8 h (Fig. 2d). These results suggest that PAR/OVA possesses a strong propensity for endosomal escape in DCs. Given the coordinated release profiles of OVA and R837, along with the endosomal escape capability of the carrier, the PAR/OVA nanovaccine effectively enhanced the cytosolic delivery of both components. This coordinated delivery is crucial for the efficient activation of BMDCs and antigen cross-presentation.

Prior to a comprehensive evaluation using cellular and animal assays, the biocompatibility of the vaccine was assessed. After 24 h of treatment with various concentrations of PAR NPs or PAR/OVA, cell viability was assessed using the CCK-8 assay. As illustrated in Fig. 2e and Fig. S5 (supplementary information), PAR NPs showed mild cytotoxicity within a specific concentration range, whereas the incorporation of OVA significantly improved the cellular biocompatibility of the vaccine.

3.3 In vitro DC maturation and cross-presentation assay

DC activation is crucial in antigen presentation, initiating adaptive immunity against tumors. Previous studies have shown that targeting TLRs promotes DC maturation in

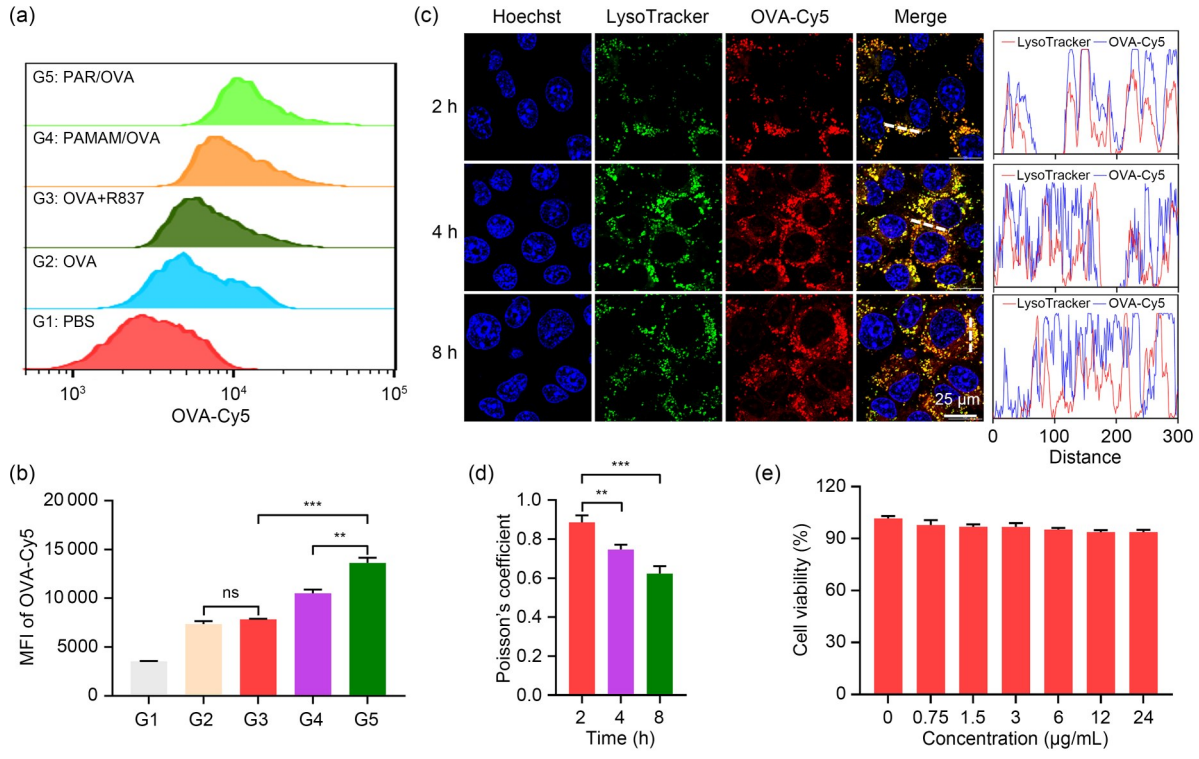

Fig. 2 Cellular uptake and intracellular localization of OVA. (a) Flow cytometric analysis of cellular uptake of different OVA formulations after a 4-h incubation. (b) Quantitative analysis of the mean fluorescence intensity (MFI) of OVA-Cy5 in DC2.4 cells pretreated with various OVA formulations for 4 h. (c) Confocal fluorescence images of DC2.4 cells treated with PAR/OVA-Cy5 for 2, 4, and 8 h, along with fluorescence intensity distribution profiles for LysoTracker Green and OVA-Cy5. (d) Poisson's coefficient for colocalization analysis of green and red fluorescence in DC2.4 cells treated with PAR/OVA-Cy5 for 2, 4, and 8 h. (e) Cell viability of DC2.4 cells treated with various concentrations of PAR/OVA for 24 h. Data are presented as mean±standard deviation (n=3). Statistical significance was determined using a one-way ANOVA. ns: nonsignificance. $^{**}P<0.01$, $^{***}P<0.001$

murine and human models. To assess the impact of R837 on DC maturation and activation, we analyzed the phenotype of primary murine BMDCs, focusing on the expression of costimulatory markers CD80 and CD86, which indicate BMDC maturation and closely reflect the in vivo state of DCs. Our results showed that after treatment with PAR/OVA for 24 h, approximately 55.2% of BMDCs were $CD86^{+}CD80^{+}$ BMDCs, significantly higher than those treated with OVA (29.4%), PAMAM/OVA (38.2%), or OVA+R837 (44.8%) (Figs. 3a and 3b). This indicates that adding R837 effectively stimulated DC activation. After extending the incubation period to 48 h, the proportion of mature DCs in the PAR/OVA-treated group increased to 67.8%, further confirming the effectiveness of the PAR/OVA nanovaccine in activating the immune response.

To examine antigen cross-presentation in BMDCs, we treated BMDCs with different vaccine formulations and analyzed the OVA-specific peptide-positive BMDCs using flow cytometry. The results showed that OVA alone produced negligible proportions of OVA-specific peptide-positive DCs compared to those in the PBS group. Conversely, treatments with PAMAM/OVA and OVA+R837 for 48 h resulted in approximately 7.0% and 5.4% of BMDCs displaying OVA-specific peptides, respectively. However, treatment with PAR/OVA significantly increased the proportion of OVA-specific peptide-positive DCs to 15.0% (Fig. 3c), indicating that PAR/OVA can enhance antigen presentation. Additionally, the PAR/OVA nanovaccine induced the highest level of proinflammatory cytokine secretion, including TNF-α and IL-6 (Figs. 3d and 3e).

Subsequently, we examined the in vivo immune responses triggered by nanovaccine in lymph nodes, with the vaccination timeline shown in Fig. 3f. Initially, we assessed the delivery efficiency of PAR/OVA to the lymph nodes. Lymph nodes were excised and analyzed using flow cytometry 24 h after subcutaneous administration of different vaccine formulations. Figure 3g illustrates that following PAR/OVA treatment, OVA-Cy5 exhibited a significantly higher MFI in the lymph nodes than those in other formulations, highlighting the superior lymph node trafficking capability of the nanovaccine. Furthermore, flow cytometry analysis revealed that the proportion of mature DCs in the lymph nodes after treatment with PAR/OVA reached approximately 29.7%, 2.7 times that of the treatment with OVA alone (Fig. 3h). Overall, these findings indicate that PAR/OVA elicited a robust immune response.

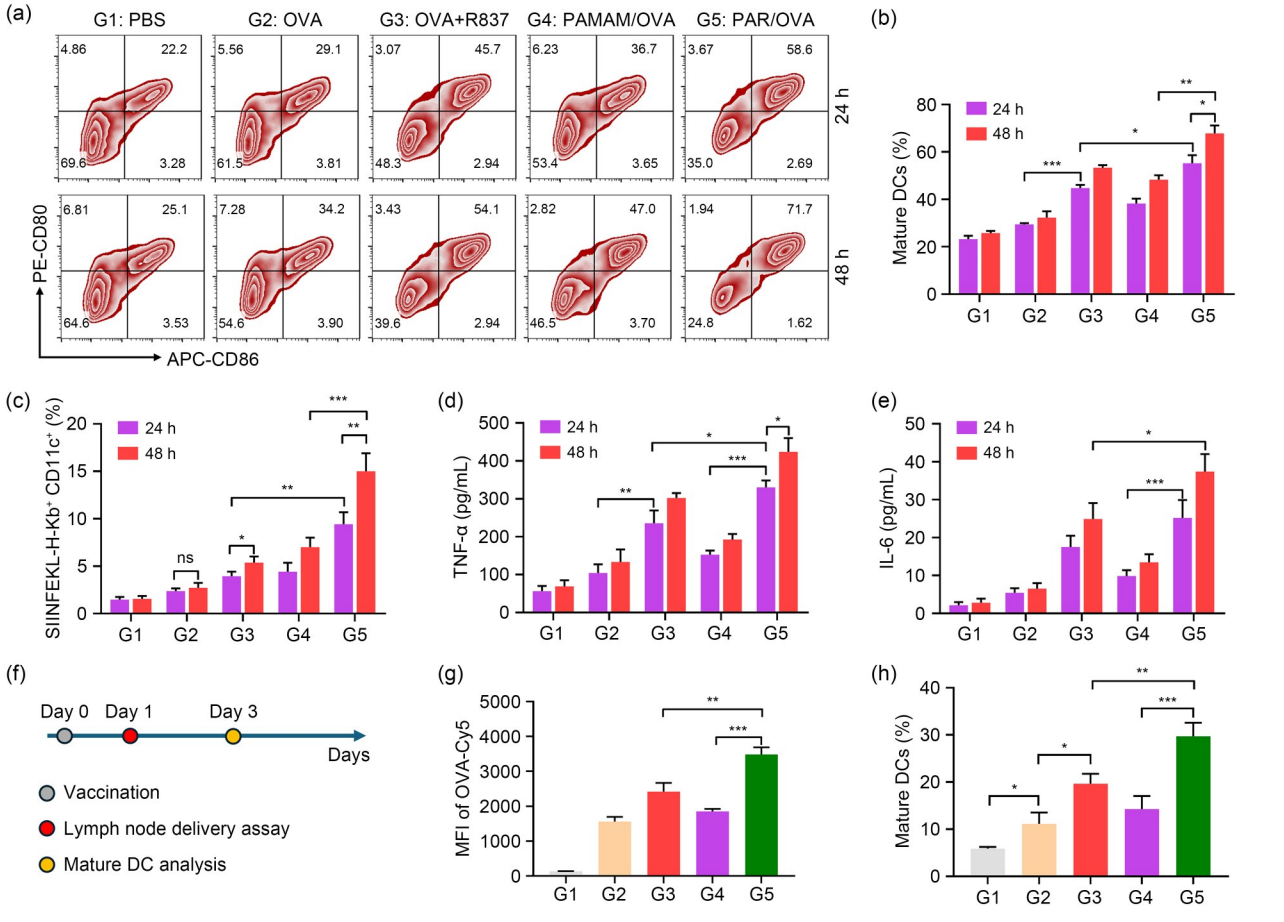

Fig. 3 DC maturation and cross-presentation assay. Representative flow cytometric images (a) and corresponding quantification (b) of mature DCs ($CD11c^+CD80^+CD86^+$) after stimulation with various OVA formulations. (c) Percentage of OVA-specific peptide-positive BMDCs following treatment with various OVA formulations. Levels of TNF-α (d) and IL-6 (e) in the supernatants of BMDCs subjected to various treatments. (f) Schematic illustration of the treatment schedule. (g) Quantitative analysis of the MFI of OVA-Cy5 in DCs in lymph nodes following various treatments. (h) Percentage of mature DCs in lymph nodes following treatment with various OVA formulations. Data are presented as mean±standard deviation (n=3). Statistical significance was determined using a one-way ANOVA. ns: nonsignificance. $^{*}P<0.05$, $^{**}P<0.01$, $^{***}P<0.001$

3.4 Prophylactic and therapeutic trials of nanovaccines

The prophylactic efficacy of the PAR/OVA nanovaccine was assessed in a B16-OVA melanoma tumor model. Mice in each experimental group received three doses of 50 μg OVA and 15.6 μg R837 per immunization (Fig. 4a). Subsequently, the mice were challenged with B16-OVA cells on Day 0, and tumor volumes were measured every 2 d. As shown in Fig. 4b, treatment with PAR/OVA significantly extended the latency period for tumor formation, whereas immunization with OVA or PAMAM/OVA resulted in negligible tumor growth inhibition (Fig. 4c; Fig. S6 in the supplementary information). Conversely, immunization with OVA+R837 resulted in moderate tumor growth inhibition. Notably, treatment with PAR/OVA nanovaccine significantly inhibited B16-OVA tumor progression, indicating that it elicited a strong protective immune response against B16-OVA melanoma. To highlight the differences in tumor volume across the groups, we photographed the mice after the treatment period (Fig. 4d). The PAR/OVA group exhibited the lowest tumor volumes, indicating significant antitumor efficacy.

The primary goal of tumor vaccines is to induce long-lasting and targeted immune responses against tumors. A key component of this process is the generation of memory T cells, vital for establishing effective immune memory. Memory T cells are classified into two types based on their phenotype and biological function: effector memory T cells (T_{EM}) and central memory T cells (T_{CM}). T_{EM}, marked by $CD44^+CD62L^-$, can rapidly respond to antigen re-exposure and migrate to peripheral tissues. In contrast, T_{CM}, characterized by $CD44^+CD62L^+$, are predominantly located in secondary lymphoid organs, serving as a long-lasting reservoir for immune defense with enhanced proliferative potential upon re-encounter with antigens [30–33].

To assess the immune memory response triggered by the nanovaccine, we euthanized the vaccinated mice and harvested their splenocytes for memory T cell analysis. In mice

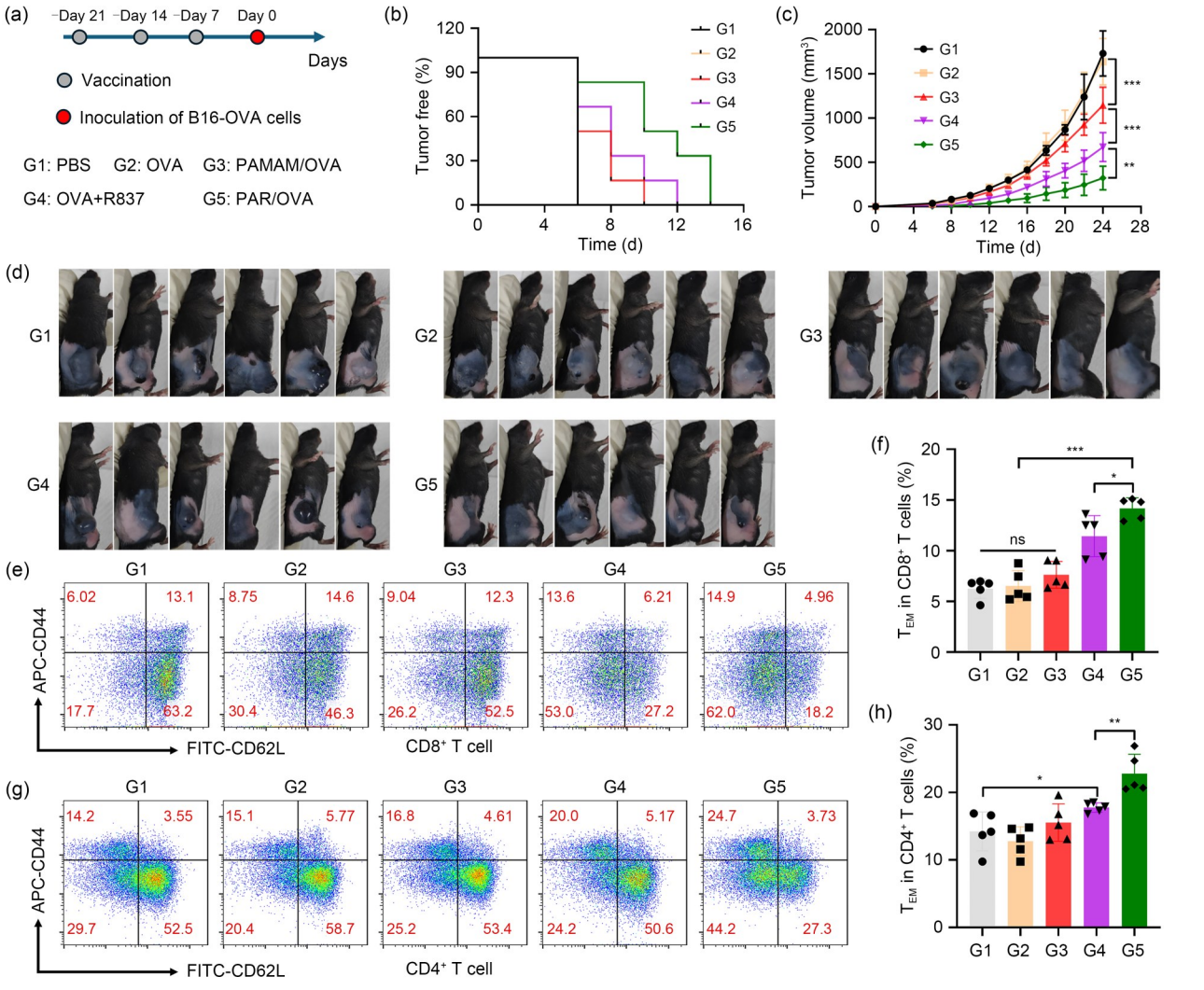

Fig. 4 Prophylactic trials of nanovaccines. (a) Schematic illustration of the treatment schedule. (b) Frequency of tumor-free mice after vaccination with various formulations and subsequent subcutaneous rechallenge with B16-OVA tumor cells. (c) Relative tumor volumes (normalized to Day 0) of mice following different treatments. (d) Representative images of mice from each group after treatment. (e) Representative flow cytometric analysis of $CD8^+$ memory T cells in lymphocytes. (f) Percentage quantification of effector memory T cells ($CD44^+CD62L^-$) within $CD8^+$ T cells. (g) Flow cytometric analysis of $CD4^+$ memory T cells in lymphocytes. (h) Percentage quantification of effector memory T cells ($CD44^+CD62L^-$) within $CD4^+$ T cells. Data are presented as mean±standard deviation (n=5). Statistical significance was determined using a one-way ANOVA. ns: nonsignificance. $^*P<0.05$, $^{**}P<0.01$, $^{***}P<0.001$

treated with PAR/OVA, the proportion of T_{EM} within the $CD8^+$ T cells increased significantly compared to other groups (Figs. 4e and 4f). This enhanced immune response suggests that PAR/OVA nanovaccine provides strong protection, enabling the immune system to more efficiently counter tumor cells with the same antigen. This effect is likely due to the enhanced activation of DCs and the efficient antigen cross-presentation facilitated by PAR/OVA. Conversely, the proportion of T_{CM} decreased significantly (Fig. S7a in the supplementary information), likely because T_{CM} rapidly differentiated into T_{EM} upon stimulation with the same antigen, thereby enhancing tumor cell elimination. $CD4^+$ memory T cells are essential for supporting the activation and function of both $CD8^+$ T cells and other immune system components. As shown in Figs. 4g and 4h and Fig. S7b (supplementary information), $CD4^+$ memory T cells exhibited a similar trend, with increased T_{EM} and decreased T_{CM} following immunization with PAR/OVA. These results indicate that treatment with PAR/OVA induces a strong immune memory response, effectively preventing tumor development and inhibiting tumor growth.

To assess the potential of the cancer vaccines against established tumors, we tested the PAR/OVA nanovaccine in a B16-OVA tumor model. B16-OVA cells were inoculated on Day 0, and the mice received subcutaneous injections of PBS, OVA, PAMAM/OVA, OVA+R837, or PAR/OVA on Days 6, 13, and 20 (Fig. 5a). As shown in Figs. 5b and 5c, neither OVA nor PAMAM/OVA significantly inhibited tumor

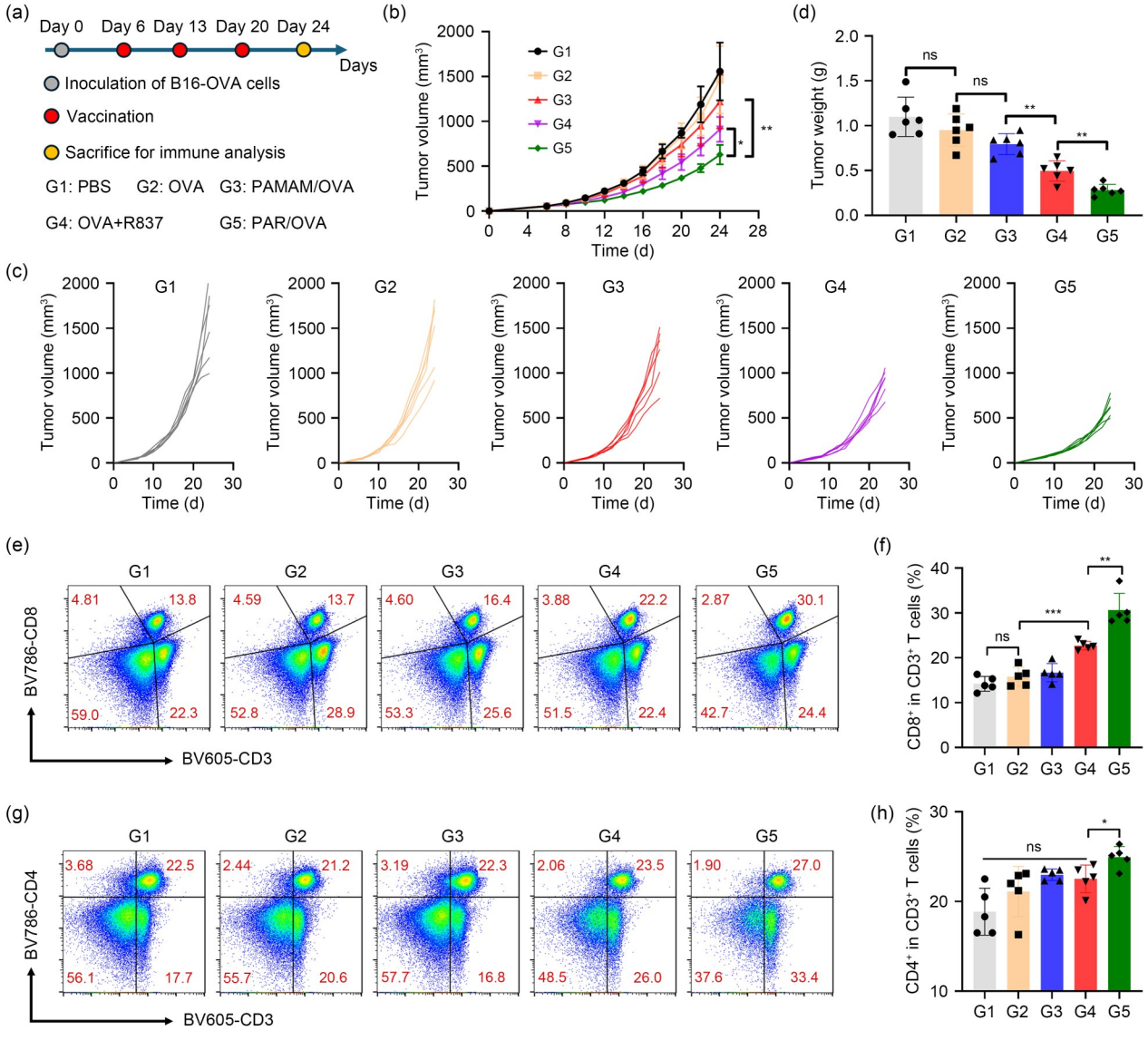

Fig. 5 Therapeutic trials of nanovaccines. (a) Schematic illustration of the treatment schedule. (b) Relative tumor volumes (normalized to Day 0) of mice following different treatments. (c) Average tumor growth curves for mice subjected to different treatments. (d) Tumor weights at the end of the antitumor study following different treatments. Representative flow cytometric analysis (e) and corresponding percentage quantification (f) of $CD8^+$ T cells in tumor-infiltrating leukocytes. Representative flow cytometric analysis (g) and corresponding percentage quantification (h) of $CD4^+$ T cells in tumor-infiltrating leukocytes. Data are presented as mean±standard deviation (n=5). Statistical significance was determined using a one-way ANOVA. ns: nonsignificance. $^*P<0.05$, $^{**}P<0.01$, $^{***}P<0.001$

growth, with no marked difference compared to the control group. Conversely, treatment with OVA+R837 resulted in moderate tumor growth inhibition, indicating a limited therapeutic effect. However, treatment with PAR/OVA significantly inhibited tumor growth, demonstrating its strong antitumor efficacy. This pronounced inhibition of tumor progression by PAR/OVA highlights its potential as an effective therapeutic agent in cancer treatment. Tumor volume differences between the groups were further confirmed by photographing and weighing the solid tumor tissues at the end of the treatment period. The PAR/OVA group exhibited the lowest tumor weight (Fig. 5d), confirming its potent antitumor efficacy. These findings were corroborated by the tumor images (Fig. S8 in the supplementary information), which showed a significant reduction in tumor size.

To determine whether treatment with PAR/OVA modified the immune cell composition of the tumor microenvironment and enhanced systemic antitumor immune responses, we examined various immune cells within the tumor tissues. As shown in Figs. 5e–5h, treatment with PAR/OVA significantly increased the proportion of $CD8^+$ T cells from 14.2% to 30.6% and $CD4^+$ T cells from 18.9% to 24.9% in the tumor tissues. These results indicate that treatment with PAR/OVA markedly reversed immunosuppression in the tumor

microenvironment and activated the antitumor immune response, confirming its potent ability to induce the anticancer immune response.

Cytokines in the tumor microenvironment play a pivotal role in cancer immunotherapy by regulating innate and adaptive immune responses, enhancing T cell activity, and promoting tumor cell apoptosis. To assess the systemic immune response triggered by the PAR/OVA nanovaccine, we quantified key cytokine levels using ELISA. Treatment with PAR/OVA resulted in a significant increase in T cell-derived cytokines, including TNF-α, interferon-gamma, and IL-6 (Figs. S9a–S9c in the supplementary information). This increase indicates a potent antitumor immune response characterized by DC activation and significant cytotoxic T lymphocyte infiltration, further supporting the efficacy of treatment with PAR/OVA in inducing robust antitumor immunity.

Furthermore, treatment with PAR/OVA had no impact on body weight (Fig. S10 in the supplementary information). To assess its systemic safety, hematological indices were evaluated seven days following treatment with PAR/OVA. Liver function was assessed by quantifying alanine aminotransferase, aspartate transaminase, and alkaline phosphatase, while kidney function was assessed by blood urea levels. Furthermore, total cholesterol and blood glucose levels were examined to monitor lipid and glucose metabolism. As shown in Fig. S11 (supplementary information), all hematological indices showed no significant differences compared to the PBS group. These findings indicate that treatment with PAR/OVA had mild side effects, supporting its potential safety for therapeutic use.

3.5 Therapeutic study in combination with αPD-1

Although ICB has significantly improved the survival of patients with cancer, long-term therapeutic responses are only observed in a minority of cases, likely due to insufficient immune cell infiltration. Since PAR/OVA effectively stimulates a strong $CD8^+$ T cell response, we combined PAR/OVA and αPD-1 to investigate their synergistic antitumor effects. As shown in Fig. 6a, mice were randomly assigned to four groups—PBS, PAR/OVA, αPD-1, and PAR/OVA+αPD-1. They received three vaccine doses (20 μg OVA per mouse) on Days 6, 13, and 20, along with intravenous injections of αPD-1

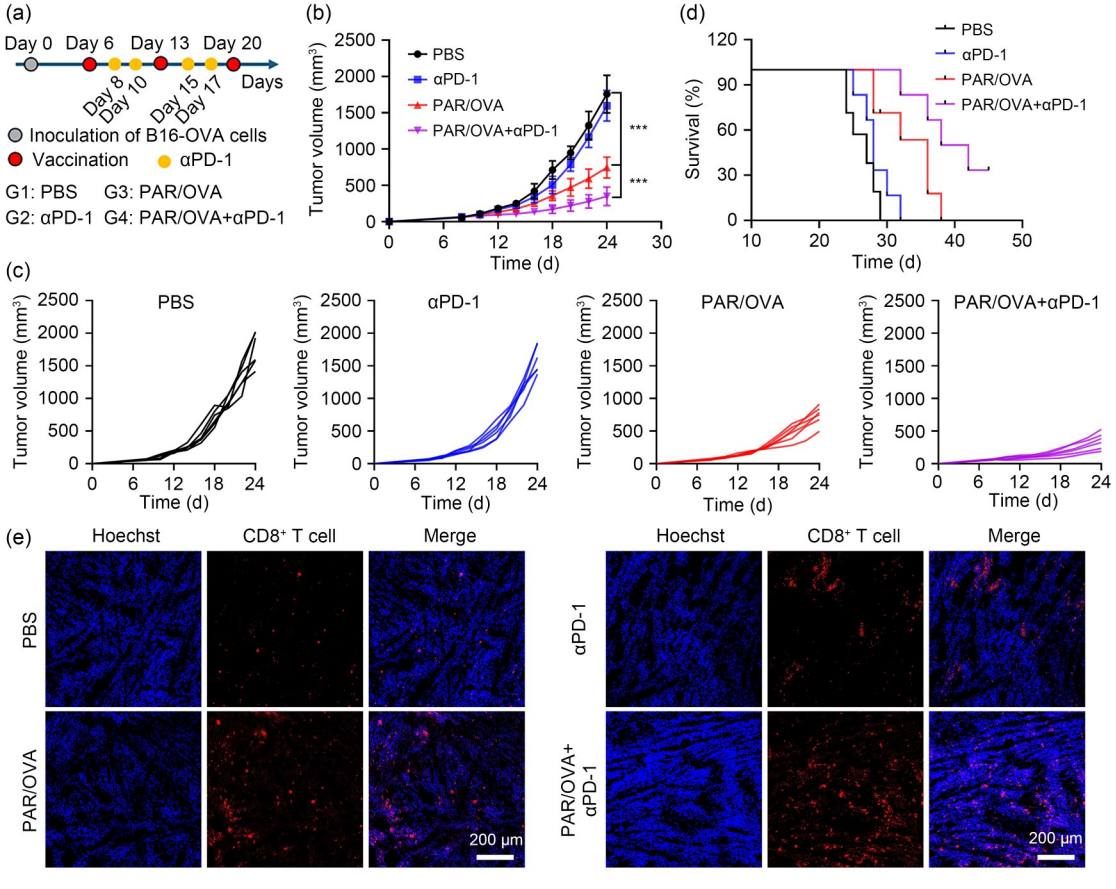

Fig. 6 Therapeutic study in combination with αPD-1. (a) Schematic illustration of the treatment schedule. (b) Relative tumor volumes (normalized to Day 0) of mice following different treatments. (c) Average tumor growth curves of mice following different treatments. (d) Survival curves of mice following different treatments. (e) Representative immunofluorescence images of $CD8^+$ T cell infiltration in tumor tissues following different treatments. Data are presented as mean±standard deviation (n=5). Statistical significance was determined using a one-way ANOVA. $^{***}P<0.001$

(20 μg per mouse) on Days 8, 10, 15, and 17. Figures 6b and 6c show that treatment with αPD-1 alone had minimal impact on tumor growth, likely due to the low injection dose. Treatment with PAR/OVA significantly reduced tumor growth. Notably, treatment with PAR/OVA+αPD-1 exhibited superior therapeutic efficacy by suppressing tumor growth. Survival rates were also significantly improved in the combination therapy group. All mice in the PBS and αPD-1 groups died within 32 d, while those in the PAR/OVA group survived for approximately 38 d. Notably, 40% of the mice in the PAR/OVA+αPD-1 group survived for 42 d (Fig. 6d). This extended survival is likely due to the ability of PAR/OVA to significantly enhance $CD8^+$ T cell infiltration into tumor tissues, while αPD-1 blocks PD-1 signaling on $CD8^+$ T cells, thereby preventing immune escape by PD-L1-overexpressing tumor cells (Fig. 6e; Fig. S12 in the supplementary information). In summary, combining PAR/OVA with αPD-1 significantly enhances antitumor efficacy and survival compared to either treatment alone, highlighting the potential of this combination therapy for more effective cancer immunotherapy.

4 Conclusions

In this study, we developed the PAR/OVA nanovaccine by combining an R837-modified PAMAM dendrimer with OVA to enhance the delivery of both antigens and adjuvants at the subcellular level. The PAMAM dendrimer endows the nanovaccine with an excellent loading capacity for R837 and OVA while facilitating the lysosomal escape of OVA and enabling cross-presentation. R837 acts as an adjuvant for the TLR7 pathway and as a structural agent that aids in OVA loading. In vitro studies showed that the PAR/OVA nanovaccine enhanced the uptake of OVA and R837 by antigen-presenting cells and promoted the escape of OVA and R837 into the cytoplasm. High cytoplasmic GSH levels triggered the breakdown of PAR/OVA, releasing OVA and R837, thereby activating DCs and facilitating antigen cross-presentation. In vivo studies showed that PAR/OVA effectively activated DCs in lymph nodes, enhanced antigen presentation, and stimulated T cell activation and proliferation, resulting in strong antitumor immune responses. Moreover, the nanovaccine exhibited enhanced antitumor efficacy through synergistic interaction with ICB, resulting in tumor growth suppression. The design of this nanovaccine offers a novel strategy for the spatiotemporal codelivery of antigens and adjuvants, thereby presenting a promising approach to cancer immunotherapy.

Our study has several limitations. First, although the PAR/OVA nanovaccine showed strong antitumor effects in preclinical mouse models, its clinical application may encounter challenges, including immune-related side effects and requiring dose optimization. As R837 is a potent immunoadjuvant, high doses could lead to excessive inflammation and adverse reactions. Therefore, optimizing the grafting density of R837 on the PAMAM is crucial. Further research should focus on exploring the structural properties, stability, and immunogenicity of PAR/OVA with varying R837 grafting densities to strike an effective balance between efficacy and safety in tumor immunotherapy. Last, although the combination of PAR/OVA with ICB shows promising antitumor effects, its clinical application requires further exploration. For example, assessing the synergy between PAR/OVA and other ICB, such as anti-PD-1, anti-CTLA-4, or novel agents targeting the tumor microenvironment, will offer valuable insights into its broader therapeutic potential. Additionally, combining PAR/OVA with other immunotherapies, such as CAR-T cell therapy or oncolytic virus treatments, may further enhance its therapeutic efficacy.

In summary, the PAR/OVA nanovaccine offers a promising approach to cancer immunotherapy by efficiently delivering antigens and adjuvants via the PAMAM dendrimer platform. R837 exhibits a dual function by serving as both an immune adjuvant and a structural component of the vaccine, thereby boosting immune activation. However, for successful clinical translation, optimizing the R837 grafting density is crucial to balance immune activation with safety. Future research should focus on overcoming challenges related to immune side effects, dose optimization, and the development of personalized therapeutic strategies.

Supplementary Information The online version contains supplementary material available at https://doi.org/10.1631/bdm.2400339.

Acknowledgements This work was supported by the Guangdong Medical Science and Technology Research Fund Project (Nos. A2022124 and B2023148), the Guangdong Provincial Administration of Traditional Chinese Medicine Research Project (No. 20231222), the National Natural Science Foundation of China (No. 52403185), Guangdong Basic and Applied Basic Research Foundation (No. 2023A1515011493), the Open Fund of Guangdong Provincial Key Laboratory of Spine and Spinal Cord Reconstruction (No. 2023B121203001), and the National Famous Old Traditional Chinese Medicine Experts Inheritance Studio Construction Program of the National Administration of TCM (No. (2022) 75).

Author contributions TSL, BKH, JQT, and KWW performed the experiments, collected the data, and conducted the data analysis and interpretation. TSL and SYH wrote the manuscript. KWW and HF generated the concept and designed the study. KWW, NLF, and HF were involved in writing, critical editing, and proofreading the manuscript.

Declarations

Conflict of interest The authors declare that they have no conflict of interest.

Ethical approval All animal experiments were conducted in accordance with the National Research Council's Guide for the Care and Use of Laboratory Animals and approved by the Animal Ethics Committee of the Animal Experimental Center of Guangdong Pharmaceutical University (Approval No. SPF2017673).

Data availability The data that support the findings of this study are available from the corresponding authors upon reasonable request.

References

1. Baruch EN, Youngster I, Ben-Betzalel G et al (2021) Fecal microbiota transplant promotes response in immunotherapy-refractory melanoma patients. Science 371(6529):602–609. https://doi.org/10.1126/science.abb5920
2. Gao WT, Wang XY, Zhou Y et al (2022) Autophagy, ferroptosis, pyroptosis, and necroptosis in tumor immunotherapy. Signal Transduct Target Ther 7(1):196. https://doi.org/10.1038/s41392-022-01046-3
3. Morris EC, Neelapu SS, Giavridis T et al (2022) Cytokine release syndrome and associated neurotoxicity in cancer immunotherapy. Nat Rev Immunol 22(2):85–96. https://doi.org/10.1038/s41577-021-00547-6
4. Ribas A (2015) Releasing the brakes on cancer immunotherapy. N Engl J Med 373(16):1490–1492. https://doi.org/10.1056/nejmp1510079
5. van der Burg SH, Arens R, Ossendorp F et al (2016) Vaccines for established cancer: overcoming the challenges posed by immune evasion. Nat Rev Cancer 16(4):219–233. https://doi.org/10.1038/nrc.2016.16
6. Saxena M, van der Burg SH, Melief CJM et al (2021) Therapeutic cancer vaccines. Nat Rev Cancer 21(6):360–378. https://doi.org/10.1038/s41568-021-00346-0
7. Blass E, Ott PA (2021) Advances in the development of personalized neoantigen-based therapeutic cancer vaccines. Nat Rev Clin Oncol 18(4):215–229. https://doi.org/10.1038/s41571-020-00460-2
8. Barbier AJ, Jiang AY, Zhang P et al (2022) The clinical progress of mRNA vaccines and immunotherapies. Nat Biotechnol 40(6):840–854. https://doi.org/10.1038/s41587-022-01294-2
9. Kuai R, Ochyl LJ, Bahjat KS et al (2017) Designer vaccine nanodiscs for personalized cancer immunotherapy. Nat Mater 16(4): 489–496. https://doi.org/10.1038/nmat4822
10. Lu YC, Shi YY, You J (2022) Strategy and clinical application of up-regulating cross presentation by DCs in anti-tumor therapy. J Contr Release 341:184–205. https://doi.org/10.1016/j.jconrel.2021.11.011
11. Gao ZL, Xu W, Zheng SJ et al (2023) Orchestrated cytosolic delivery of antigen and adjuvant by manganese ion-coordinated nanovaccine for enhanced cancer immunotherapy. Nano Lett 23(5): 1904–1913. https://doi.org/10.1021/acs.nanolett.2c04970
12. Wang KW, Yang Y, Xue W et al (2018) Cell penetrating peptide-based redox-sensitive vaccine delivery system for subcutaneous vaccination. Mol Pharm 15(3):975–984. https://doi.org/10.1021/acs.molpharmaceut.7b00905
13. Wei JY, Xue W, Yu XF et al (2017) pH sensitive phosphorylated chitosan hydrogel as vaccine delivery system for intramuscular immunization. J Biomater Appl 31(10):1358–1369. https://doi.org/10.1177/0885328217704139
14. Song T, Liao Y, Zuo QH et al (2022) MnO_2 nanoparticles as a minimalist multimode vaccine adjuvant/delivery system to regulate antigen presenting cells for tumor immunotherapy. J Mater Chem B 10(18):3474–3490. https://doi.org/10.1039/d1tb02650j
15. Zhang S, Lv J, Gao P et al (2021) A pH-responsive phase-transition polymer with high serum stability in cytosolic protein delivery. Nano Lett 21(18):7855–7861. https://doi.org/10.1021/acs.nanolett.1c03031
16. Wong KH, Guo ZP, Law MK et al (2023) Functionalized PAMAM constructed nanosystems for biomacromolecule delivery. Biomater Sci 11(5):1589–1606. https://doi.org/10.1039/d2bm01677j
17. Hu JJ, Hu K, Cheng YY (2016) Tailoring the dendrimer core for efficient gene delivery. Acta Biomater 35:1–11. https://doi.org/10.1016/j.actbio.2016.02.031
18. Chen ZY, Peng YT, Li YC et al (2021) Aptamer-dendrimer functionalized magnetic nano-octahedrons: theranostic drug/gene delivery platform for near-infrared/magnetic resonance imaging-guided magnetochemotherapy. ACS Nano 15(10):16683–16696. https://doi.org/10.1021/acsnano.1c06667
19. Xu J, Wang H, Xu LG et al (2019) Nanovaccine based on a protein-delivering dendrimer for effective antigen cross-presentation and cancer immunotherapy. Biomaterials 207:1–9. https://doi.org/10.1016/j.biomaterials.2019.03.037
20. Bhagchandani S, Johnson JA, Irvine DJ (2021) Evolution of Toll-like receptor 7/8 agonist therapeutics and their delivery approaches: from antiviral formulations to vaccine adjuvants. Adv Drug Deliv Rev 175:113803. https://doi.org/10.1016/j.addr.2021.05.013
21. Sun MY, Liu ZW, Wu L et al (2023) Bioorthogonal-activated in situ vaccine mediated by a COF-based catalytic platform for potent cancer immunotherapy. J Am Chem Soc 145(9):5330–5341. https://doi.org/10.1021/jacs.2c13010
22. Zhang LR, Zhang JJ, Xu LX et al (2021) NIR responsive tumor vaccine in situ for photothermal ablation and chemotherapy to trigger robust antitumor immune responses. J Nanobiotechnol 19(1):142. https://doi.org/10.1186/s12951-021-00880-x
23. Jiang F, Ding BB, Liang S et al (2021) Intelligent MoS_2-CuO heterostructures with multiplexed imaging and remarkably enhanced antitumor efficacy via synergetic photothermal therapy/chemodynamic therapy/immunotherapy. Biomaterials 268:120545. https://doi.org/10.1016/j.biomaterials.2020.120545
24. Shou YH, Yang L, Yang YS et al (2021) Inhibition of keratinocyte ferroptosis suppresses psoriatic inflammation. Cell Death Dis 12(11):1009. https://doi.org/10.1038/s41419-021-04284-5
25. Lynn GM, Laga R, Darrah PA et al (2015) In vivo characterization of the physicochemical properties of polymer-linked TLR agonists that enhance vaccine immunogenicity. Nat Biotechnol 33(11):1201–1210. https://doi.org/10.1038/nbt.3371
26. Chen Q, Xu LG, Liang C et al (2016) Photothermal therapy with immune-adjuvant nanoparticles together with checkpoint blockade for effective cancer immunotherapy. Nat Commun 7(1): 13193. https://doi.org/10.1038/ncomms13193
27. Xiong X, Zhao JY, Pan JM et al (2021) Personalized nanovaccine coated with calcinetin-expressed cancer cell membrane antigen for cancer immunotherapy. Nano Lett 21(19):8418–8425. https://doi.org/10.1021/acs.nanolett.1c03004
28. Zhou BQ, Wu Q, Wang M et al (2020) Immunologically modified $MnFe_2O_4$ nanoparticles to synergize photothermal therapy and immunotherapy for cancer treatment. Chem Eng J 396:125239. https://doi.org/10.1016/j.cej.2020.125239
29. Liu T, Zhu M, Chang XW et al (2023) Tumor-specific photothermal-therapy-assisted immunomodulation via multiresponsive adjuvant nanoparticles. Adv Mater 35(18):2300086. https://doi.org/10.1002/adma.202300086
30. Wang KW, Jiang ML, Li T et al (2024) A synergistic chemoimmunotherapy system leveraging PD-L1 blocking and bioorthogonal prodrug activation. Adv Mater 36(30):2402322. https://doi.org/10.1002/adma.202402322

31. Wang KW, Xiao X, Jiang ML et al (2021) An NIR-fluorophore-based theranostic for selective initiation of tumor pyroptosis-induced immunotherapy. Small 17(36):2102610. https://doi.org/10.1002/smll.202102610
32. Liu LX, Ma PC, Wang H et al (2016) Immune responses to vaccines delivered by encapsulation into and/or adsorption onto cationic lipid-PLGA hybrid nanoparticles. J Contr Release 225:230–239. https://doi.org/10.1016/j.jconrel.2016.01.050
33. Guo Z, Li S, Qu YC et al (2021) Bio-membrane adhesive poly(choline phosphate L-glutamate)-based nanoparticles as vaccine delivery systems for cancer immunotherapy. Chem Eng J 417:127970. https://doi.org/10.1016/j.cej.2020.127970